Development of a Conceptual Design of a Fixed Wing Unmanned Aerial Vehicle for Intelligence, Surveillance and Reconnaissance

EDWARD JOSEPH M. BAUTISTA[1], DR. RODANTE G. FLORES[2]
[1, 2] *Philippine State College of Aeronautics – Institute of Graduate Studies*

Abstract- ***This study aims to develop a first-pass analysis of the conceptual design of a fixed-wing unmanned aerial vehicle for intelligence, surveillance, and reconnaissance missions, which aims to encourage the development of locally made designs and bolster the capability of our nation to monitor and defend its own territory and natural resources. To come up with the conceptual design, the researcher used readily available resources and tools from existing literature for ease of replication of the design project for future researchers. The estimations are done using an up-to-date statistical curve fit equation, which gives an accurate estimation of the final design specifications. The result of the study is used to catalyze research interest pertaining to unmanned aerial vehicle design and utilize drone technology currently available for the benefit of mankind and national development.***

Indexed Terms- Drone, Unmanned Aerial Vehicle, Conceptual Design, ISR

I. INTRODUCTION

At the onset of rapid technological advancement for the past decade, the potential application of unmanned aerial vehicles has been highlighted to do more of the labor-intensive and risky tasks usually performed manually. In the present context, unmanned aerial vehicles have a wide range of applications such as environmental monitoring, disaster response, mapping, recreation, entertainment industry, and other civilian and military applications such as intelligence, reconnaissance, and surveillance (ISR) and intelligence, reconnaissance, target acquisition, and reconnaissance (ISTAR). In comparison, intelligence, reconnaissance, and surveillance (ISR) is the process of gathering information about a target area or an adversary, while intelligence, reconnaissance, target acquisition, and reconnaissance (ISTAR) adds the ability to target and engage targets within the identified target area, which includes individuals, facilities, and other crucial equipment on the front lines.

Since most of the functions are similar, drones developed for this particular application can be used to collect imagery to identify targets, assess damage, and track movements through the use of high-resolution cameras or specialized cameras that can penetrate and see through the target area. In addition, these drones can also be equipped with sensors to collect intelligence signals, such as radio and radar signals used for identifying enemy forces, tracking their movements, and intercepting their communication. Moreover, the drones can also conduct long-term surveillance on the target area to monitor enemy activity, identify potential threats, and gather intelligence on enemy capabilities. Once these functions have been performed by the drones, the operator can now decide and weigh out the option of targeting and engaging enemy forces in the target area, such as through air strikes, air support, or the elimination of high-value targets.

Based on the defined function and usefulness of drones used for intelligence, surveillance, and reconnaissance, regardless of whether they are equipped with a target function or not, these drones can be both a tool for protection and a weapon on the front lines. According to an article published by New America, the use of drones can be compared with the introduction of tanks during World War I which took years to be incorporated into the frontlines as a new mobile-armored warfare weapon. Furthermore, the researcher can provide the same analogy and insight on the future of drones for future warfare, given the changing appetite of the world for traditional warfare.

During early integration and development in the military, drones were expected to prove their worth in war using the early-developed unmanned aircraft systems for counter-insurgency missions such as the war in Afghanistan and Iraq, where they earned their badge on the practical uses of more cost-effective drones in the future. In the context of the ongoing Ukraine-Russia war, the use of unmanned aerial vehicles, or drones, has solidified and established its importance and advantage over traditional warfare. Counter-offensive measures have been more efficient and cost the operators less burdens financially and less casualties since they can be used as both an eye in the sky and a weapon for counterattacks on the frontlines. It is undeniable that employing drones has greatly affected the results of the war, and it is a subject area of debate regarding the significant role of drones for various missions and domains. In addition, not only sophisticated drones specialized for intelligence, surveillance, and reconnaissance were used in the war, but also available drones are commonly used for recreation and other various civilian applications. These commercial off-the-shelf (COTS) drones were used and modified to perform the functions of other specialized drones, commonly called loitering munitions, for one-way mission purposes. These so-called loitering munitions are making their way into the integration of technology in existing military fleets with even more precise accuracy and availability, which is also a subject in the changing appetite for war for future applications. With cost of development and technological advancement as an initial driving factor, unmanned aerial vehicles have been a less popular option for practical applications in both civilian and military settings in the past decades. This is why they are commonly used for recreational purposes; a remotely piloted unmanned aerial vehicle has become a top choice for civilian enthusiasts. Drones, together with sophisticated and costly equipment, are increasingly being integrated into risky and vital operations that are typically handled by human pilots due to the rapid growth of technology.

The purpose of this study is to develop a conceptual design for a fixed-wing UAV that can be used for intelligence, surveillance, and reconnaissance mission requirements, which could account for limited excess of payload for future upgrades and cater to the dynamic demand of future mission requirements.

II. PROCEDURE

- Research Design

This study aims to generate design variables based on the established mission requirements for the unmanned aerial vehicle to come up with an initial working sketch for the conceptual design. In this study, a quantitative approach derived from existing literature was employed. The data used for approximations were results from currently available sources such as published journals and literature in order to attain realistic results based on the accuracy of data from existing designs.

- Design Process

The study started by establishing a mission specification (or mission profile) for the conceptual unmanned aerial vehicle design. The mission specification is a depiction of how the aircraft will perform its mission from takeoff to landing from one point to another. After the mission profile, a comparative analysis of existing unmanned aerial vehicle in the market was done to establish a realistic performance requirement for the design. Additional requirements in terms of payload were also included to ensure that the unmanned aerial vehicle design would be capable to perform its intended function. At this point of the design process, these parameters were identified clearly and realistically as this would serve as a basis for the succeeding results of the design process.

After establishing the performance requirements, an initial sizing procedure was conducted to determine the maximum takeoff weight or design gross weight of the unmanned aerial vehicle design using methods presented by Raymer, D. P. (2006) and the statistical equations representing up to date historical data of similar unmanned aerial vehicle designs presented by Finger, D. F. (2016). The procedure for determining an initial estimate for the design gross weight used historical data presented by Raymer, D. P. (2006) for weight fractions and the following sizing equation for iteration:

$$W_o = W_{payload} + W_{autopilot} + W_{fuel} + W_{empty} \qquad (eq.1)$$

The next procedure involves constructing a power loading versus wing loading diagram with the expected performance requirements acting as constraint lines to identify a good design point for the optimal wing loading and power loading. These parameters dictate the size of the wing and the size of powerplant that could cater for the established performance requirements. The following equations presents different performance constraint lines for necessary phases of flight:

$$\left(\frac{W}{S}\right)_{V_{stall}} = \frac{1}{2}\rho V_s^2 C_{L_{max}} \qquad (eq.2)$$

$$\left(\frac{W}{P}\right)_{V_{max}} = \frac{\eta_p}{0.5\frac{\rho_o V_{max}^3 C_{do1}}{\left(\frac{W}{S}\right)} + \frac{2K}{\rho\sigma V_{max}}\left(\frac{W}{S}\right)} \qquad (eq.3)$$

$$\left(\frac{W}{P}\right)_{S_{TO}} = \frac{1-\exp\left(0.6\rho g C_{D_G} S_{TO}\frac{1}{\left(\frac{W}{S}\right)}\right)}{\mu-\left(\mu+\frac{C_{D_G}}{C_{L_R}}\right)\left[\exp\left(0.6\rho g C_{D_G} S_{TO}\frac{1}{\left(\frac{W}{S}\right)}\right)\right]}\left(\frac{\eta_p}{V_{TO}}\right) \qquad (eq.4)$$

$$\left(\frac{W}{P}\right)_{ROC} = \frac{1}{\frac{ROC}{\eta_p} + \sqrt{\frac{2}{\rho\sqrt{\frac{3C_{Do}}{K}}}\left(\frac{W}{S}\right)}\left(\frac{1.155}{\left(\frac{L}{D}\right)_{max}\eta_p}\right)} \qquad (eq.5)$$

$$\left(\frac{W}{P}\right)_{C} = \frac{\sigma_C}{\frac{ROC_c}{\eta_p} + \sqrt{\frac{2}{\rho_c\sqrt{\frac{3C_{Do}}{K}}}\left(\frac{W}{S}\right)}\left(\frac{1.155}{\left(\frac{L}{D}\right)_{max}\eta_p}\right)} \qquad (eq.6)$$

$$BHP = \frac{W_o}{(W/P)} \qquad (eq.7)$$

$$S_{wing} = \frac{W_o}{(W/S)} \qquad (eq.8)$$

After the constraint diagram was constructed, an optimal design point was identified by inspecting intersections of more than two constraint lines. In addition, an optimal design point was identified as the value of the wing loading and power loading which would in turn give the largest wing area and largest engine available. This would ensure that the aircraft would be capable to provide lift and power in all mission segments the unmanned aerial vehicle was designed to undergo.

Once the wing area and the engine horsepower was determined, calculations for the aircraft geometry were done using methods presented by Raymer, D. P. (2006), Sadraey, M. H. (2013) and Götten et al. (2018) using the following equations for each component respectively:

Component No. 1: Wing

$$AR = \frac{b^2}{S} \qquad (eq.9)$$

$$\lambda = \frac{c_{tip}}{c_{root}} \qquad (eq.10)$$

$$MAC = \frac{2}{3}c_{root}\left(\frac{1+\lambda+\lambda^2}{1+\lambda}\right) \qquad (eq.11)$$

$$L = W_o \qquad (eq.12)$$

Component No. 2: Fuselage

$$L_{fuselage} = aW_o^C \qquad (eq.13)$$

$$d_{fuselage_{max}} = 1.2816 * 10^{-9}(m_o)^3 - 2.5110 * 10^{-6}(m_o)^2 + 1.5465 * 10^{-3}(m_o) + 7.1638 * 10^{-2} \qquad (eq.14)$$

Component No. 3: Empennage or Tail

The empennage sizing was fundamentally similar to the wing. Therefore, the tail geometry was computed using the same equations for sizing the wing. In addition, historical values presented as tail volume coefficients as presented by Raymer, D. P. (2006) and Sadraey, M. H. (2013) served as an initial indicator of how the aircraft will behave in terms of its stability, control and trim. However, since conceptual design is inherently an iterative process, this value would be subject to revisions based on the performance requirements set in the initial phases of the design and other external factors which will influence the performance requirements as intended by the designer. Therefore, a first pass analysis was conducted and other design iterations will be performed once an initial computation for stability is available.

Component No. 4: Landing Gear

$$d_{tire} = AW_w^B \qquad (eq.15)$$

$$w_{tire} = AW_w^B \qquad (eq.16)$$

Lastly, construction of a working sketch for the conceptual design of the unmanned aerial vehicle was done based on the designer's experience and considerations to ensure that it would result in a practical design. In addition, the working sketch would serve as a basis for the estimation of aerodynamic drag of the unmanned aerial vehicle design. The resulting value for aerodynamic drag represents the drag of the unmanned aerial vehicle due to its shape or its profile drag. In future studies, this value would serve as a reference value for performance calculations to be used for design optimization to ensure that the most

optimal design would be selected. This was done using the component method presented by Raymer, D. P. (2006) using the following equations:

$$C_{L_\alpha} = \frac{2\,\pi\,AR}{2+\sqrt{4+\frac{AR^2\beta^2}{\eta^2}\left(1+\frac{\tan\Lambda^2_{\max}}{\beta^2}\right)}}\left(\frac{S_{exposed}}{S_{wing}}\right)(F) \qquad (eq.17)$$

$$RN = \frac{\rho V l}{\mu} \qquad (eq.18)$$

$$RN_{cutoff} = 38.21\left(\frac{l}{k}\right)^{1.053} \qquad (eq.19)$$

For wing, tail, struts and pylons:

$$FF = \left[1+\frac{0.6}{\left(\frac{x}{c}\right)_m}\left(\frac{t}{c}\right)+100\left(\frac{t}{c}\right)^4\right][1.34M^{0.18}cos\Lambda_m^{0.28}] \qquad (eq.20)$$

For fuselage and smooth canopy:

$$FF = 1+\frac{60}{f^3}+\frac{f}{400} \qquad (eq.21)$$

For nacelle and external store:

$$FF = 1+\frac{0.35}{f} \qquad (eq.22)$$

$$f = \frac{l}{d} \qquad (eq.23)$$

For cooling drag:

$$\frac{D}{q_{cooling}} = 4.9*10^{-7}\left(\frac{BHP*T^2}{\sigma V}\right) \qquad (eq.24)$$

For miscellaneous engine drag:

$$\frac{D}{q_{miscellaneous}} = 2*10^{-4}*BHP \qquad (eq.25)$$

III. RESULTS

Mission Specification and Performance Requirements

The conceptual design of unmanned aerial vehicle was expected to operate conforming to a simple mission profile as depicted by the figure below to perform intelligence, surveillance and reconnaissance missions.

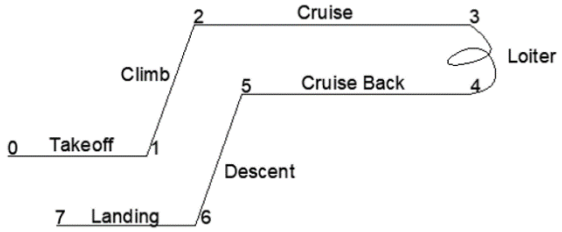

Figure. 1
Mission Specification

Based on the comparative analysis of similar unmanned aerial vehicle for intelligence, surveillance and reconnaissance missions, the following performance requirements are established:

Stall Speed (V_{stall})	35 knots
Maximum Speed (V_{max})	120 mph
Cruising Speed (V_{cruise})	108 mph
Loiter Speed (V_{loiter})	156 mph
Max. Rate of Climb (ROC_{max})	500 ft/min
Takeoff Run ($S_{takeoff}$)	200 ft
Service Ceiling (h_{sc})	11000 ft
Range (R)	100 km
Endurance (E)	12 hrs.

Gross Weight Estimation

In reference to figure 1, each mission segment has an estimated weight fraction based on statistical data presented by Raymer, D. P. (2006) and Sadraey, M. H. (2013). The following data is presented below. The mission segment for cruise, loiter, and cruise back, which is basically the range and endurance of the unmanned aerial vehicle, was estimated using the simplified Breguet's equation of range and endurance, respectively.

Takeoff	W_1/W_o	0.98
Climb	W_2/W_1	0.97
Cruise	W_3/W_2	0.993
Loiter	W_4/W_3	0.703
Cruise Back	W_5/W_4	0.993
Descent	W_6/W_5	0.99
Landing	W_7/W_6	0.997
Total Mission Segment Weight Fraction	W_7/W_o	0.6504

Figure 2.
Mission Segment Weight Fractions

In addition to the mission segment weight fractions, there is a set payload requirement of 150 lbs. It was set by the designer to carry munitions, weapon systems,

and specialized equipment intended to meet the intended mission requirements. Furthermore, an autopilot weighing 30 lbs. was also added for future upgrades of the electronics installed intended for the operation of the unmanned aerial vehicle. With these parameters identified, a sizing procedure was conducted through iteration with the addition of using an empty weight fraction estimation of the unmanned aerial vehicle using the working equation presented by Finger, D. F. (2016), which covered a population of unmanned aerial vehicles of a range of sizes and weights. Incorporation of this statistical curve fit equation ensures accuracy and reliability of the results falling within the range of the regression analysis in terms of weight. The following results are presented based on the iteration procedure conducted for initial sizing:

$W_{o\ guess}$ (N)	$W_{calculated}$ (N)	Difference	m_o (D.F. Finger)			
4503.7	4503.714259	100.0003%	459.25339	kg	1012.475	lbs.
4503.71	4503.712954	100.0001%	459.25325	kg	1012.475	lbs.
4503.72	4503.711648	99.9998%	459.25312	kg	1012.475	lbs.
4503.73	4503.710342	99.9996%	459.25299	kg	1012.475	lbs.
4503.74	4503.709037	99.9993%	459.25285	kg	1012.474	lbs.
4503.75	4503.707731	99.9991%	459.25272	kg	1012.474	lbs.
4503.76	4503.706426	99.9988%	459.25259	kg	1012.474	lbs.

Figure 3.
Design Gross Weight Iteration

The table provides data pertaining to the guess weight and calculated weight of the unmanned aerial vehicle, which should show convergence and serve as the selected design gross weight of the vehicle. A difference of 99.9998% was the result, which gives the guess weight and the calculated weight the smallest difference. Therefore, a weight of 4,503.71 N (459.25 kg, 1012.474 lb_m) would be selected as the design gross weight (MTOW) of the unmanned aerial vehicle based on the payload weight, autopilot weight, range, and endurance requirements set by the designer.

Wing Loading and Power Loading Selection

Figure 4.
Constraint Diagram

From figure 4, the following concepts should be established to interpret the graph. The performance constraint lines in terms of the maximum speed, takeoff run, rate of climb, and ceiling requirements for the aircraft were presented as a function of both power loading and wing loading. Each curve graphed above has a desirable region under each graph. This means that an optimal value lies at the intersection of these desirable regions. In addition, the maximum speed is only a function of wing loading and is graphed using a broken red line, which has a desirable region on the left-hand side of the graph. Using the intersections of the performance requirements, the following data is observed: First, the optimal design point lies in the area that should give us the biggest engine (lowest power loading) and the biggest wing area (smallest wing loading), provided that at least two or more of these performance requirements intersect. The optimal design point was shown by the green circle, as given by the data above. These give a value for the power loading of 6.48 lb/HP and a value for the wing loading of 5.81 lb/ft^2. Using the results from the design gross weight estimation, the following parameters were identified:

S_{wing} = 174.298 ft^2 [Wing Area]
BHP = 156.126 HP [Engine Power]

The parameters identified should be inferred as the adequate wing area that could provide the lift that covers the entire mission segment of the mission specification of the unmanned aerial vehicle design. Furthermore, the engine horsepower that would satisfy the thrust requirements in the entire range of the mission segment should be 156.126 HP. For the sake of discussion, a typical Cessna 172 engine gives about 140 HP up to around 160 HP in some variations. With existing engines on the market, it will not be difficult to procure a 160 HP engine, which is more than enough for prototyping this unmanned aerial vehicle, rendering it more cost-effective rather than resorting to the development of experimental engines.

Wing Design

After the wing area was identified, the wing design procedure was started using initial inputs from the methods presented by Raymer, D. P. (2006) and Sadraey, M. H. (2013). Furthermore, in order to determine the optimal airfoil that would provide enough lift for the unmanned aerial vehicle design, it

was therefore necessary to perform an airfoil selection from maximum lift coefficient versus ideal lift coefficient presented by Sadraey, M. H. (2013). The ideal lift coefficient computed was 0.3, and the maximum lift coefficient for the aircraft design was around 1.5. From the figure, the following airfoil sections capable of producing these values are identified to be NACA 23012, NACA 23015, NACA 23018, and NACA 23024. The airfoil selection process would therefore focus on the characteristics presented by the following airfoil section until an optimal design and ideal aerodynamic characteristics were established.

Airfoil Section	C_{dmin}	C_{mo}	AOA_{stall}	AOA_0	cl/cd_{max}	Stall Quality
NACA 23012	0.006	-0.024	18	-1.9	128.2051	Sharp
NACA 23015	0.0065	-0.02	18	-1.2	110	Docile
NACA 23018	0.007	-0.03	16	-1.8	122.2222	Moderate
NACA 23024	0.0083	-0.018	15.6	-1.7	76.92308	Moderate

Figure 5.
Airfoil Selection

The parameters from the airfoil data presented by Abott (2020), gave the reference values presented in the table provided in figure 5. It is important to look at two things for this design, which are the maximum airfoil efficiency and the stall quality of the airfoil design. As indicated by the comparison, it is desirable to have a moderate stall quality for the airfoil; however, it would be at the expense of the airfoil efficiency, which is an indicator of the set range and endurance. Given the case, the designer opted to use the airfoil, which produces the maximum airfoil efficiency, at the expense of the stall quality of the unmanned aerial vehicle. This compromise was made because, all throughout the flight duration of the conceptual aircraft, it should, at the very least, fly autonomously, which could be programmed to avoid stalling the aircraft accurately. Therefore, it ensured that the unmanned aerial vehicle is aerodynamically efficient to meet its intended range for cruising and its intended endurance for loitering in the course of its mission.

From the data presented by Raymer, D. P. (2006), the dihedral angle for an unswept low wing design was chosen to be 5 degrees, and a sweep angle was set to 0 degrees. Other geometries, which are presented below, were computed using MATLAB code. The goal of iterating the values for these geometric parameters was to ensure that an elliptical lift curve distribution would be achieved by the wing design through the application of lifting line theory. The resulting wing geometric parameters should result in a wing design with minimum drag due to lift using conventional wing planforms, mitigating difficulties in manufacturing or prototyping. The result of these computations and the theoretical lift distribution are presented below:

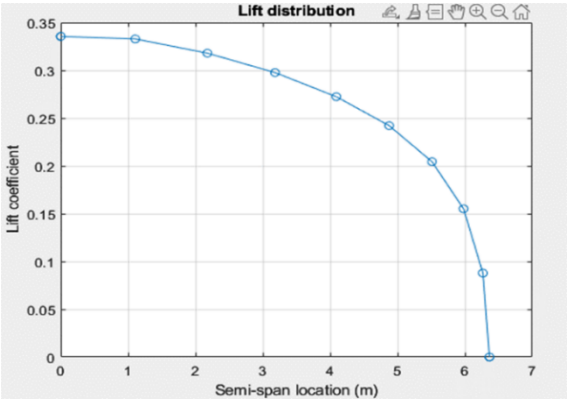

Figure 6.
Spanwise Elliptical Lift Distribution

NACA 23012	MATLAB	
i_{wing}	2	deg
a_{twist}	-2	deg
Aspect Ratio	10	
C_{L_a}	6.20	/rad
a_0	-1.9	deg
λ	0.7	
b	41.75	ft
MAC	4.17	ft
C_{root}	4.86	ft
C_{tip}	3.40	ft

Figure 7.
Wing Geometric Parameters from MATLAB

Fuselage Design

The fuselage parameters were computed using the methods presented by Raymer, D. P. (2006) and Götten et al. al. (2018). The procedure conducted was based on the design gross weight of the aircraft and the assumed classification of the conceptual design, which was homebuilt. The computed fuselage length was 17.191 ft. and has a fuselage design based on the geometry of an ellipse. The calculated maximum fuselage diameter is based on the methods presented by Götten et al. (2018) was 2.561 ft., which could cater

for a 160 HP engine, for its indicated payload for intelligence, surveillance, and reconnaissance missions, and for a dedicated autopilot weight. It was imperative to give consideration for the maximum height of the engine in order for the powerplant to be integrated to the fuselage with ease.

Empennage Design

The tail design parameters were computed using the methods presented by Raymer, D. P. (2006), and Sadraey, M. H. (2013). The procedure conducted was similar for the wing design, except for the moment arm computation and the inclusion of the tail volume coefficient for the sizing of the tail areas. The tail volume coefficient is a non-dimensional coefficient that relates the tail geometry to the wing geometry. As presented by Raymer, D. P. (2006) and Sadraey, M. H. (2013), the estimation of tail volume coefficients ensures that an adequate tail size for the design was determined to effectively perform its intended function. The tail volume coefficient selected was 0.5 for the horizontal tail and 0.04 for the vertical tail, respectively. The following tail design parameters are shown below:

Geometric Parameter	Horizontal Tail	Vertical Tail
Aspect Ratio	4	1.5
λ_{tail}	0.4	0.4
S	42.33 ft^2	33.86 ft^2
b	13.01 ft	7.13 ft
$C_{root_{tail}}$	4.65 ft	6.79 ft
$C_{tip_{tail}}$	1.86 ft	2.72 ft
MAC_{tail}	3.45 ft	5.04 ft
Y_{MAC}	2.79 ft	3.05 ft
$l_{arm_{tail}}$	8.60 ft	
$l_{tailboom}$	7.77 ft	
$d_{tailboom}$	0.31 ft	

Figure 8.
Tail Geometric Parameters

From the results presented in the table above, the moment arm of the tail is less than three times the value of its mean aerodynamic chord, rendering the aircraft as a short-coupled design aircraft. This would mean that excessive size and deflection of the tail control surfaces are required for the tail to perform its functions. For a first pass analysis, the design was considered since at this aspect of the design, a stability analysis was not yet conducted, which means that a revision to the geometry of the tail would be inevitable later on in the optimization process. Furthermore, the need for prototyping, wind tunnel testing, flight testing, and stability analysis would give the designer the need to revise the tail geometries to satisfy an intended stability requirement for the aircraft. Thus, for any design procedure, the tail geometry would be subject to revision on the basis of sizing the tail areas based on performance requirements and/or stability requirements.

Landing Gear Design

The landing gear design parameters are based on the procedures presented by Raymer, D. P. (2006), which estimate the optimal tire diameter and width for the main gear and the nose gear of the unmanned aerial vehicle. These data were computed since the weights carried by these sections are different. It was stated by Raymer, D. P. (2006) that at least 85% of the design gross weight should be carried by the main landing gear, and the remaining 15% should be carried by the nose gear. Therefore, the following results based on sizing procedures are presented below:

	Diameter (in)	Width (in)
Main Landing Gear	15.97	5.89
Nose Landing Gear	8.72	3.43

Figure 9.
Landing Gear Geometric Parameters

Drag Coefficient Calculation

After determining the geometries of the major component of the conceptual unmanned aerial vehicle design, the following sketch is provided below as a result of the computations made by the designer.

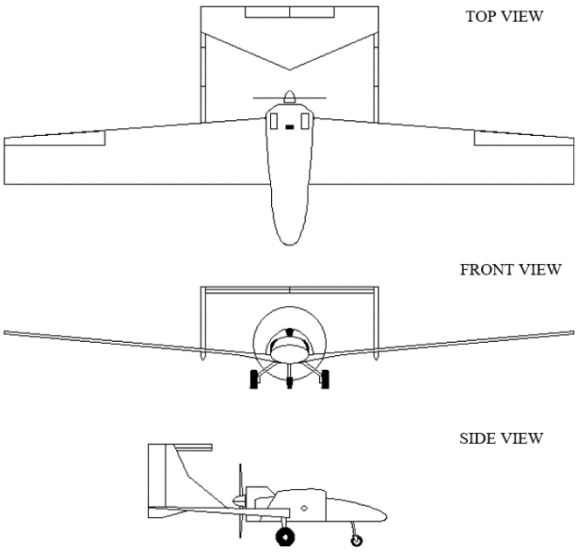

From the sketch presented above, the designer selected an unconventional aircraft configuration since the aircraft would not carry a human payload when performing its mission. This means that the designer is flexible enough to alter the fuselage geometry based on the payload it is required to carry. In addition, since the powerplant would not impede the loaded payload, it was positioned near the center of gravity of the fuselage to minimize disruptions over the wing through the propeller wash and to minimize flow separation and boundary layer buildup in the fuselage. Furthermore, since the powerplant is of a pusher configuration, the designer resorted to an unconventional twin-tail boom design to position the structure away from the propeller and to position the tail surfaces away from the propeller wash.

Finally, the drag characteristics of the conceptual design were computed using the methods presented by Raymer, D. P. (2006). Utilizing the conceptual sketch in computer-aided drafting and design software, the required reference areas were computed using the software feature and served as a basis for the estimation of the overall drag of the conceptual design. The following results are presented for each component drag of the conceptual design:

Component	Drag Coefficient
Fuselage	0.00315
Wing	0.00920
Horizontal Tail	0.00226
Vertical Tail	0.00092
Tail Boom	0.00027
Landing Gear	0.00299
Cooling	0.00018
Miscellaneous (Engine)	0.00018
Total	0.02070

Figure 10.
Drag Coefficient for Major Components

The results presented in the table above represent the breakdown of the drag of the component, which is 0.02. The relevance of the coefficient of drag is that most of the resisting force that should be overcome by the thrust of the aircraft is directly related to the total drag of the aircraft, which is mainly due to its profile and the drag as a result of lift production. The resulting drag from the table pertains to the profile drag, which constitutes a significant portion of the total drag of the aircraft. Therefore, from these results, we could infer that the conceptual design has a higher aerodynamic efficiency as compared with common manned aircraft designs because its profile drag is lower than typical designs with a value of 0.03 as presented by Raymer, D. P. (2006) and Sadraey, M. H. (2013) in their estimations.

ACKNOWLEDGMENT

I would like to extend my heartfelt gratitude to everyone who have supported and contributed in the completion of this thesis. The journey to this milestone was challenging and rewarding, and I could not have reached this point without the help and encouragement of many remarkable individuals.

First and foremost, I would like to express my gratitude to God, our Creator, through his never-ending grace and mercy for providing the necessary patience, knowledge and understanding to get through the process as a grown and matured individual.

To my thesis adviser, Prof. Rodante G. Flores, Ph. D., I express my deepest appreciation for his unwavering commitment to see through the outcome of this research with his expertise and mentorship all

throughout the research process. His feedback, insights, experience and dedication have been instrumental in shaping the direction of this study. I am truly grateful for his patience and encouragement which has helped me to strive for excellence.

To the panel members of the Institute of Graduate Studies, Dr. Estrella E. Yago, Dr. Eleonor H. Calayag, Dr. Gil Brian O. Santos, Dr. Leonardo C. Medina Jr. and Dr. Roderick C. Santiago, who have shared their wisdom and time to guide and steer the direction of the study which made the accomplishment of this paper possible.

Lastly, special thanks to my family, friends, peers from the Faculty of Aeronautical Engineering, my loved ones and the love of my life for the unconditional love and support. Their belief in my abilities and their encouraging words have been a fuel to keep me going despite the difficulties I have encountered along the way. I am forever grateful for their sacrifices and understanding in this journey.

REFERENCES

[1] Davies, P. H. J. (2021). ISR versus ISTAR: A Conceptual Crisis in British Military Intelligence. International Journal of Intelligence and Counterintelligence, 35(1), 73–100. https://doi.org/10.1080/08850607.2020.1866334

[2] Raymer, D. P. (2006). Aircraft design: A conceptual approach. Reston, Va.: American Institute of Aeronautics and Astronautics. ISBN: 1563478293

[3] Sadraey, M. (2020). Design of Unmanned Aerial Systems (1st ed.). Wiley. Retrieved from https://www.perlego.com/book/1425846/design-of-unmanned-aerial-systems-pdf (Original work published 2020)

[4] Sadraey, M. H. (2013). Aircraft design: A systems engineering approach. Chichester: John Wiley and Sons. ISBN: 9781118352700

[5] Singhal, Gaurav & Bansod, Babankumar & Mathew, Lini. (2018). Unmanned Aerial Vehicle Classification, Applications and Challenges: A Review. 10.20944/preprints201811.0601.v1.

[6] Shakhatreh, Hazim & Sawalmeh, Ahmad & Al-Fuqaha, Ala & Dou, Zuochao & Almaitta, Eyad & Khalil, Issa & Othman, Noor & Khreishah, Abdallah & Guizani, Mohsen. (2019). Unmanned Aerial Vehicles (UAVs): A Survey on Civil Applications and Key Research Challenges. IEEE Access. 7. 48572 - 48634. 10.1109/ACCESS.2019.2909530.

[7] Chase, M. S. (2015, March 12). Emerging trends in China's development of unmanned systems. RAND. https://www.rand.org/pubs/research_reports/RR990.html

[8] Boulanin, Vincent & Verbruggen, Maaike. (2017). Availability and military use of UAVs.

[9] Banks, R. L., & Al, A. C. a. S. C. M. A. (n.d.). The Integration of Unmanned Aerial Vehicles into the Function of Counterair. In DTIC. https://apps.dtic.mil/sti/citations/ADA381841

[10] Volovelsky, Uri. (2014). Civilian uses of unmanned aerial vehicles and the threat to the right to privacy – An Israeli case study. Computer Law & Security Review. 30. 306–320. 10.1016/j.clsr.2014.03.008.

[11] Xie, Y., Savvarisal, A., Tsourdos, A., Zhang, D., & Gu, J. (2021). Review of hybrid electric powered aircraft, its conceptual design and energy management methodologies. Chinese Journal of Aeronautics, 34(4), 432–450. https://doi.org/10.1016/j.cja.2020.07.017

[12] Varsha, N & Somashekar, V. (2018). Conceptual design of high performance Unmanned Aerial Vehicle. IOP Conference Series: Materials Science and Engineering. 376. 012056. 10.1088/1757-899X/376/1/012056.

[13] Sobester, Andras & Keane, Andy & Scanlan, James & Bressloff, Neil. (2005). Conceptual Design of UAV Airframes Using a Generic Geometry Service. 10.2514/6.2005-7079.

[14] Finger, D.. (2016). Comparative Performance and Benefit Assessment of VTOL and CTOL UAVs.

[15] Götten, Falk & Finger, D. & Braun, Carsten & Havermann, Marc & Bil, Cees & Gómez, Francisco. (2018). Empirical Correlations for Geometry Build-Up of Fixed Wing Unmanned Air Vehicles.

[16] Dimayuga, R. G., II, & Ca, N. P. S. M. (n.d.). COTS Drone Design: a rapid equipage alternative for force recon companies. In DTIC. https://apps.dtic.mil/sti/citations/AD1126864

[17] Tahir, A., Böling, J. M., Haghbayan, M., Toivonen, H., & Plosila, J. (2019). Swarms of Unmanned Aerial Vehicles — A Survey. Journal of Industrial Information Integration, 16, 100106. https://doi.org/10.1016/j.jii.2019.100106

[18] Wang, L., Zhao, X., Zou, Y., Wang, X., Ma, T., & Gao, X. (2021). Unmanned aerial vehicle swarm mission reliability modeling and evaluation method oriented to systematic and networked mission. Chinese Journal of Aeronautics, 34(2), 466–478. https://doi.org/10.1016/j.cja.2020.02.026

[19] Zhang, Y., Hu, Z., Wang, Z., Wen, X., & Lu, Z. (2023). Survivability Analysis of Unmanned Aerial Vehicle Network based on Dynamic Weighted Clustering Algorithm with Dual Cluster Heads. Electronics, 12(7), 1743. https://doi.org/10.3390/electronics12071743

[20] Yaacoub, J. A., Noura, H., Salman, O., & Chehab, A. (2020). Security analysis of drones systems: Attacks, limitations, and recommendations. Internet of Things, 11, 100218. https://doi.org/10.1016/j.iot.2020.100218

[21] Boukoberine, M. N., Zhou, Z., & Benbouzid, M. (2019). A critical review on unmanned aerial vehicles power supply and energy management: Solutions, strategies, and prospects. Applied Energy, 255, 113823. https://doi.org/10.1016/j.apenergy.2019.113823

[22] a bv. (2020). Theory of wing sections (H. Abott). www.academia.edu. https://www.academia.edu/43217878/Theory_of_Wing_Sections_H_Abott_

[23] Franke, U. (2023, August 11). Drones in Ukraine and beyond: Everything you need to know. ECFR. https://ecfr.eu/article/drones-in-ukraine-and-beyond-everything-you-need-to-know/#:~:text=Drones%20have%20documented%20the%20destruction,help%20direct%20and%20conduct%20strikes.

[24] Simon, S. (2023, August 5). How the use of drones in Ukraine has changed war as we know it. NPR. https://www.npr.org/2023/08/05/1192343968/how-the-use-of-drones-in-ukraine-has-changed-war-as-we-know-it

[25] Myre, G. (2023, March 28). A Chinese drone for hobbyists plays a crucial role in the Russia-Ukraine war. NPR. https://www.npr.org/2023/03/21/1164977056/a-chinese-drone-for-hobbyists-plays-a-crucial-role-in-the-russia-ukraine-war

[26] Losey, S. (2022, August 19). Lockheed working on expendable, advanced drones to team up with Air Force fighters. Defense News. https://www.defensenews.com/unmanned/2022/07/17/lockheed-working-on-expendable-advanced-drones-to-team-up-with-us-air-force-fighters/

[27] Officer, A. a. C. a. C. C. (2023). Humans vs. Automation: How More Drones Make People Safer. Percepto. https://percepto.co/humans-vs-automation-how-more-drones-make-people-safer/

[28] Monnik, M. (n.d.). Risks and Rewards of using COTS drones in the Ukraine-Russia conflict. www.linkedin.com. https://www.linkedin.com/pulse/risks-rewards-using-cots-drones-ukraine-russia-conflict-mike-monnik

[29] Freedberg, S. J., Jr, & Freedberg, S. J., Jr. (2023). Dumb and cheap: When facing electronic warfare in Ukraine, small drones' quantity is quality. Breaking Defense. https://breakingdefense.com/2023/06/dumb-and-cheap-when-facing-electronic-warfare-in-ukraine-small-drones-quantity-is-quality/

[30] Kaplan, L. (2022, April 21). Loitering munitions in Ukraine and beyond - war on the rocks. War on the Rocks. https://warontherocks.com/2022/04/loitering-munitions-in-ukraine-and-beyond/

[31] Frąckiewicz, M. (2023). Deploying drones in military operations: opportunities and challenges. TS2 SPACE. https://ts2.space/en/deploying-drones-in-military-operations-opportunities-and-challenges/

[32] Haider, L. C. A. (2022, May 9). Future threats: military UAS, terrorist drones, and the dangers of the second drone Age - Joint Air Power Competence Centre. Joint Air Power Competence Centre - NATO's Advocate to Air and Space Power. https://www.japcc.org/chapters/c-uas-future-

threats-military-uas-terrorist-drones-and-the-dangers-of-the-second-drone-age/

[33] President's Papers: The Future of Philippine Warfare Vol. 1. (2021). National Defense College of the Philippines. Retrieved June 20, 2023, from https://ndcp.edu.ph/wp-content/uploads/2022/01/PP-Future-of-Philippine-Warfare-Web.pdf